







Far-field unlabeled super-resolution imaging with superoscillatory illumination

Cite as: APL Photonics 5, 066107 (2020); <https://doi.org/10.1063/1.5144918>

Submitted: 12 January 2020 . Accepted: 20 May 2020 . Published Online: 19 June 2020

Edward T. F. Rogers , Shmma Quraishe , Katrine S. Rogers , Tracey A. Newman , Peter J. S. Smith , and Nikolay I. Zheludev 



View Online



Export Citation



CrossMark

ARTICLES YOU MAY BE INTERESTED IN

[Label-free deeply subwavelength optical microscopy](#)

Applied Physics Letters **116**, 131105 (2020); <https://doi.org/10.1063/5.0003330>

[Controlling dispersion in multifunctional metasurfaces](#)

APL Photonics **5**, 056107 (2020); <https://doi.org/10.1063/1.5142637>

[Effect of magnesium oxide adhesion layer on resonance behavior of plasmonic nanostructures](#)

Applied Physics Letters **116**, 241601 (2020); <https://doi.org/10.1063/5.0008665>

SUBMIT TODAY!



AVS Quantum Science

SPECIAL ISSUE:
Quantum Sensing and Metrology

Co-Published by



AIP
Publishing

Far-field unlabeled super-resolution imaging with superoscillatory illumination

Cite as: APL Photon. 5, 066107 (2020); doi: 10.1063/1.5144918

Submitted: 12 January 2020 • Accepted: 20 May 2020 •

Published Online: 19 June 2020



View Online



Export Citation



CrossMark

Edward T. F. Rogers,^{1,2,a)}  Shmma Quraishe,³  Katrine S. Rogers,⁴  Tracey A. Newman,³ 
Peter J. S. Smith,^{1,5,6}  and Nikolay I. Zheludev^{2,7} 

AFFILIATIONS

¹Institute for Life Sciences, University of Southampton, Highfield, Southampton SO17 1BJ, United Kingdom

²Optoelectronics Research Centre and Centre for Photonic Metamaterials, University of Southampton, Highfield, Southampton SO17 1BJ, United Kingdom

³Clinical and Experimental Sciences, Faculty of Medicine, University of Southampton, Southampton SO17 1BJ, United Kingdom

⁴School of Mathematics and Statistics, The Open University, Walton Hall, Milton Keynes MK7 6AA, United Kingdom

⁵Biological Sciences, Faculty of Natural and Environmental Sciences, University of Southampton, Southampton SO17 1BJ, United Kingdom

⁶Marine Biological Laboratory, Woods Hole, Massachusetts 02543, USA

⁷Centre for Disruptive Photonic Technologies, School of Physical and Mathematical Sciences, The Photonic Institute, Nanyang Technological University, Singapore 637371

^{a)} Author to whom correspondence should be addressed: E.T.F.Rogers@soton.ac.uk

ABSTRACT

Unlabeled super-resolution is the next grand challenge in imaging. Stimulated emission depletion and single-molecule microscopies have revolutionized the life sciences but are still limited by the need for reporters (labels) embedded within the sample. While the Veselago–Pendry “super-lens,” using a negative-index metamaterial, is a promising idea for imaging beyond the diffraction limit, there are substantial technological challenges to its realization. Another route to far-field subwavelength focusing is using optical superoscillations: engineered interference of multiple coherent waves creating an, in principle, arbitrarily small hotspot. Here, we demonstrate microscopy with superoscillatory illumination of the object and describe its underlying principles. We show that far-field images taken with superoscillatory illumination are themselves superoscillatory and, hence, can reveal fine structural details of the object that are lost in conventional far-field imaging. We show that the resolution of a superoscillatory microscope is determined by the size of the hotspot, rather than the bandwidth of the optical instrument. We demonstrate high-frame-rate polarization-contrast imaging of unmodified living cells with a resolution significantly exceeding that achievable with conventional instruments. This non-algorithmic, low-phototoxicity imaging technology is a powerful tool both for biological research and for super-resolution imaging of samples that do not allow labeling, such as the interior of silicon chips.

© 2020 Author(s). All article content, except where otherwise noted, is licensed under a Creative Commons Attribution (CC BY) license (<http://creativecommons.org/licenses/by/4.0/>). <https://doi.org/10.1063/1.5144918>

INTRODUCTION

The Abbe–Rayleigh diffraction limit of conventional optical instruments has long been a barrier to studies of microscale and nanoscale objects. The earliest attempts to overcome it recorded the evanescent field of the object: contact photography^{1,2} and scanning near-field imaging (SNOM).^{3–5} Such near-field techniques can

provide a nanoscale resolution, but capturing evanescent fields requires a probe (or photosensitive material) to be in the immediate proximity of the object. Therefore, these techniques cannot be used to image inside cells or silicon chips, for example. More recently, other techniques have been proposed to reconstruct and capture evanescent fields including the far-field Veselago–Pendry “super-lens,” which uses a slab of negative-index metamaterial as a

lens to image the evanescent waves from an object on to a camera.⁶ This approach, however, faces substantial technological challenges in its implementation in optics and has not yet been developed as a practical imaging technique.

Biological super-resolution imaging is dominated by the powerful stimulated emission depletion (STED) and single-molecule localization (SML) microscopies. These far-field techniques have demonstrated the possibility of nanoscale imaging without capturing evanescent fields,⁷ which decay over a scale of about one wavelength away from the object. These techniques, while they have become widely used, also have their limitations. Both STED and some of the SML techniques use an intense beam to excite, deplete, or bleach fluorophores in the sample. Indeed, the resolution of STED images is fundamentally linked to the intensity of the depletion beam. The damage caused by these intense beams is known as phototoxicity, as it stresses, and eventually kills, living samples. SML is also inherently slow, requiring thousands of images to be captured to build a single high-resolution image. Moreover, STED and SML require fluorescent reporters within the sample, usually achieved by genetic modification or antibody-mediated labeling with fluorescent dyes or quantum dots. Although these labels do provide a high degree of specificity, they are known to change the behavior of the molecules or biological systems being studied^{8–10} and cannot be applied to solid artificial nanostructures such as silicon chips. They also introduce a form of bias into a study: when imaging a labeled sample, you need to know in advance what part of the system displays interesting behavior. While fluorescent imaging is easier to interpret, therefore, unlabeled imaging removes the implicit bias and exposes the native biology in all its complexity.

The other major far-field super-resolution technique is structured illumination microscopy (SIM), but it can only double the resolution of a conventional microscope¹¹ and requires capture of multiple images with complex post-processing. It is, therefore, vulnerable to processing artefacts and is also conventionally applied to labeled samples. While there have been some works on unlabeled SIM,^{12,13} these require complex optical setups and algorithmic post-processing. Similar works on rotating coherent scattering microscopy^{14,15} allow unlabeled imaging without post-processing but still require complex optics and remain limited to doubling the resolution of the optical system. The interferometric scattering microscopy (iSCAT) technique^{16,17} allows unlabeled high-resolution imaging, but only works on very clean, sparse samples, making it unsuitable for cellular biological samples. Recent work using “traditional” SIM with superoscillatory grating illumination shows great promise¹⁸ provided the scaling of intensity for multilobe superoscillations can be overcome. There is also a contact near-field SIM method that provides a resolution beyond that of the far-field SIM technique.¹⁹ However, in near-field SIM, the object is placed in contact with the grating that provides structured illumination and, therefore, is not generally suitable for bioimaging. As with any other near-field technique, it is not comparable with the far-field superoscillatory imaging reported here.

Far-field super-resolution imaging is possible using light diffracted from a precisely engineered mask that creates extremely rapid spatial variations of electromagnetic fields in free space. These fields, known as superoscillations, have large local wave numbers (phase gradients), but more importantly can have foci much smaller

than allowed by the Abbe–Rayleigh limit, as was first noted by Di Francia.²⁰ Superoscillatory focusing is a particular manifestation of the more general wave phenomenon of superoscillation, which was first noted in quantum mechanics.²¹ This counter-intuitive phenomenon allows a band-limited wave to oscillate locally much faster than the highest Fourier component of the signal. The first theoretical description of optical superoscillations²² was almost concurrent with their first observation, where subwavelength hotspots were discovered in the diffraction pattern of coherent light from a quasi-crystal array of nanoholes.²³ It was quickly realized that superoscillations could be used for super-resolution imaging without evanescent fields.^{24–27} The mechanism of superoscillatory focusing is now well understood and is related to the formation of nanoscale vortices and energy backflow zones pinned to the focal area.²⁸

So far, superoscillatory imaging has only been demonstrated using sparse nanostructured binary test samples,^{25,29} and imaging of complex unlabeled biological samples has never been demonstrated. Moreover, the mechanism of creating a super-resolution image with a band-limited microscope system has not yet been explained. This raises a number of questions and challenges. How does superoscillatory illumination lead to super-resolution? Would the precise interference of multiple waves forming the superoscillatory focus be robust enough to image complex biological samples? Would light scattered from the sidebands accompanying the superoscillatory focus be sufficiently suppressed to allow for accurate direct imaging without prior knowledge of the sample? Could superoscillatory imaging be combined with a contrast technique that allows the study of unlabeled transparent biological samples? Finally, could a practical version of the microscope be developed which allows for video-rate imaging of live biological specimens?

To address these challenging questions, we built our superoscillatory microscope to allow optical beam scanning, in a reflection (or epi) configuration—speeding up acquisition and allowing a petri dish of living cells to be imaged in real time. This is done with a spatial light modulator which shapes the beam entering a high-numerical-aperture (NA) objective. We use a liquid crystal polarization controller to implement an advanced form of polarization-contrast imaging, giving a high contrast even in unstained transparent biological samples (see the [supplementary material](#) for a detailed schematic of the imaging setup).

In this paper, we demonstrate that superoscillatory microscopy can be efficiently used for imaging of living, unlabeled biological cells, and explain the underlying mechanism of superoscillatory imaging. We constructed a practical superoscillatory microscope with which we demonstrated, for the first time, that superoscillatory imaging: (1) provides a greater spatial resolution than bright-field microscopy in the same setting; (2) gives radically more information on the fine details of the object than confocal microscopy; (3) can be combined with polarization-contrast imaging for transparent objects (e.g., cells); (4) is possible at video frame rates and at low optical intensities. To illustrate these features of superoscillatory microscopy, we performed resolution tests with standard test samples and conducted the first ever *in vitro*, high-frame-rate super-resolution polarization-contrast imaging of living unlabeled biological samples (mouse bone cells and neurons).

PRINCIPLES OF SUPEROSCILLATORY MICROSCOPY

A conventional microscope uses a powerful objective lens with a high numerical aperture to project light scattered by the object (sample) to the image plane where it is registered. Typically, an incoherent light beam with a homogeneous profile is used to illuminate the object. The spatial resolution of a conventional microscope is limited by the focusing ability of the objective lens (its point spread function) and cannot exceed $\lambda/(2 \times \text{NA})$, where λ is the wavelength of the light used for imaging and NA is the numerical aperture of the objective lens used for imaging. This is known as the Abbe–Rayleigh diffraction limit of microscopy.

In superoscillatory focusing, the interference of multiple coherent waves creates a hotspot that, in principle, can be arbitrarily small. The focus of a conventional lens with a circular aperture of finite diameter is the familiar Airy pattern, with an intense hotspot in the middle surrounded by a series of rings of increasing diameter and decreasing intensity. However, a typical superoscillatory lens creates a more complex pattern with a central hotspot surrounded by a zone of low intensity known as the “field of view.” Outside this field, a broad, often high intensity, sideband, also known as the “halo,” is typically observed (see the inset in Fig. 1). However, we will show that we can work at power levels up to 100 times smaller than those of standard fluorescent confocal microscopes, meaning that the halo does not cause significant phototoxicity.

Due to the presence of the halo around a superoscillatory focus, simply replacing the conventional objective lens in a widefield microscope with a superoscillatory lens is not practical for objects that are bigger than the field of view. This is because the halo will be present in the image, distorting it. The effect of the halo can, however, be mitigated by using a superoscillatory lens for structured illumination of the sample combined with confocal detection. In this configuration, a conventional lens with a high numerical aperture is used as the objective lens, while the object (sample) is illuminated by

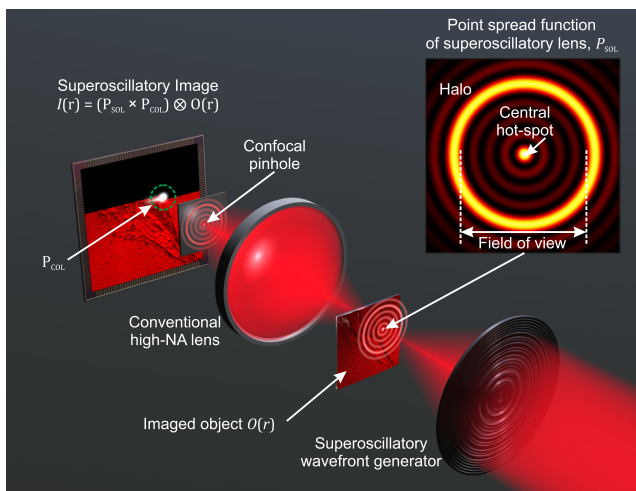


FIG. 1. Principles of microscopy with superoscillatory illumination. The figure shows a simplified layout of the microscope in transmission mode (for the layout of the epi version of the instrument see details in the [supplementary material](#)). The inset in the upper right corner shows the structure of a superoscillatory hotspot.

a superoscillatory lens with a tight focus. A small confocal aperture is used to detect only the central part of the image, thus excluding the halo. Imaging is achieved by scanning the sample relative to the focus of the superoscillatory lens. In the apparatus reported here, we implemented this configuration to improve the resolution of a conventional biological microscope with minimal modifications to the existing optics.

We now describe this configuration in more detail (see the simplified schematic of the superoscillatory microscope in Fig. 1). Let the point spread functions of the illuminating superoscillatory lens (SOL) and conventional objective lens (COL) be P_{SOL} and P_{COL} , respectively. The point spread function of the microscope is then $P_{\text{MIC}} = P_{\text{SOL}} \times P_{\text{COL}}$, while the microscope’s response remains band limited to spatial frequency $\omega_{\text{max}} = 2\pi \times \text{NA}/\lambda$, where NA is the average of the numerical apertures of the illuminating lens (SOL) and the imaging lens (COL), as in conventional confocal microscopy.³⁰ Let the object be described by function $O(\mathbf{r})$ that may have subwavelength structures: that is, $O(\mathbf{r})$ is not necessarily band limited to ω_{max} . Due to the bandwidth limitation, a conventional microscope cannot resolve fine details beyond $\lambda/(2\text{NA})$, but the superoscillatory microscope can. This is because the image $I(\mathbf{r}) = P_{\text{MIC}} \otimes O(\mathbf{r})$ is also a superoscillatory function and can, therefore, locally oscillate much faster than ω_{max} and can contain details finer than $\lambda/(2\text{NA})$. Here, the symbol \otimes denotes a convolution of the point spread function of the microscope and the object.

Therefore, the main principle of superoscillatory microscopy is that superoscillatory illumination creates a superoscillatory image. We illustrate this by a trivial example of imaging a pair of narrow infinitely long slits in an opaque screen separated by 0.36λ (one-dimensional imaging). To do this, we plot, in Figs. 2(a) and 2(b), hypothetical point spread functions of a superoscillatory illuminating lens $P_{\text{SOL}}(x)$, a conventional imaging lens $P_{\text{COL}}(x)$, and of the complete microscope system P_{MIC} . Images of the pair of slits $O(x)$ taken with conventional and superoscillatory microscopes are shown in Figs. 2(c) and 2(d), respectively. Slits separated by 0.36λ (far less than the diffraction limit of 0.5λ) are not resolved with a conventional lens and are well-resolved with superoscillatory illumination. This is possible because the image $I(x)$ itself is superoscillatory, as shown in Fig. 2(d): Superoscillatory regions where $k_{\text{local}} = \frac{d\varphi}{dx} > k_0$ are marked by vertical yellow lines. As is characteristic to superoscillatory functions, this image contains local spatial frequency components far higher than those in the global spectrum, as shown in Fig. 2(e): the global spectrum remains band limited, but the local spectrum extends into regions that are not available to confocal or structured illumination microscopes.

Before going into more detail, it is instructive to compare superoscillatory imaging and STED microscopy (see Fig. 3). STED (stimulated emission depletion microscopy) is a powerful technique for super-resolution microscopy. STED functions by depleting fluorescence in specific regions of the sample while leaving a central focal spot active to emit fluorescence. This focal area can be engineered by altering the properties of the depleting focal spot and the intensity of the depleting laser. In contrast, superoscillatory microscopy functions by illuminating the sample locally with a superoscillatory lens. Both are far-field super-resolution techniques that reconstruct the image non-algorithmically and without prior knowledge of the image by scanning a hotspot across the object. While STED requires

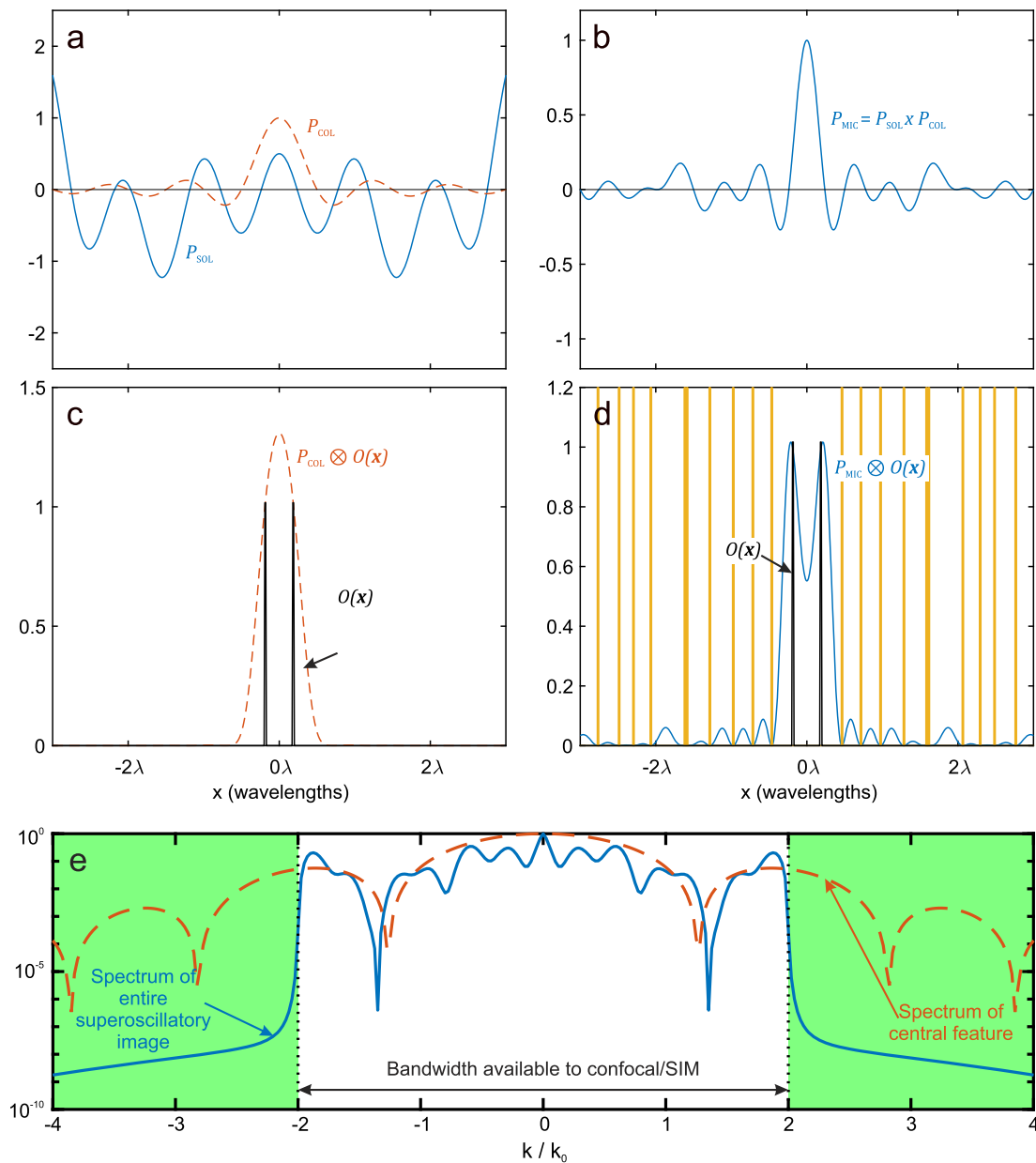


FIG. 2. Superoscillatory illumination creates superoscillatory images with sub-diffraction features. (a) Point spread functions of the illuminating superoscillatory lens P_{SOL} (blue solid line) and of the conventional imaging lens P_{COL} (orange dashed line) used in the imaging apparatus. (b) Combined point spread function P_{MIC} of the superoscillatory microscope. (c) Test object—two slits in an opaque screen— $O(x)$ (black solid line) and its brightfield image $P_{\text{COL}} \otimes O(x)$ taken with a conventional lens (orange dashed line). Slits are not resolved with a conventional lens. (d) Superoscillatory image of the slits $P_{\text{MIC}} \otimes O(x)$ resolves the slits (blue line). Superoscillatory regions with a fast variation in the phase are marked by vertical yellow lines. (e) Spatial spectra (log scale) of the entire image $P_{\text{MIC}} \otimes O(x)$ (blue solid line) and its central feature (orange dashed line). Note that the spectrum of the entire image is band limited to double the Abbe–Rayleigh limit, as it is in confocal imaging. The green region highlights the region beyond the conventional band limit of confocal imaging.

labeling of the sample with a fluorescent reporter (e.g., dye or quantum dots), superoscillatory microscopy works with unlabeled samples. STED is a nonlinear optical technique that requires intense laser radiation to deplete the fluorescence around the central focal

spot, while superoscillatory microscopy is a linear imaging technique that works at any given wavelength of light and is subject only to the same signal-to-background (or contrast) requirements as any other imaging technique.

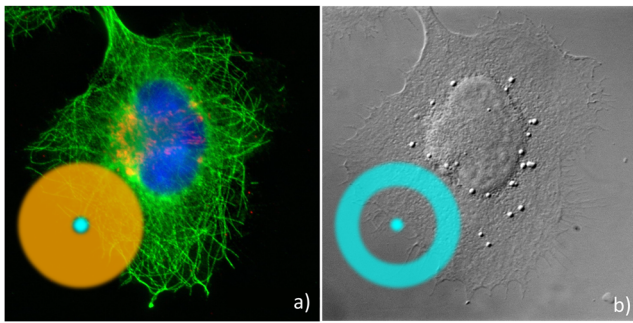


FIG. 3. Microscopy with superoscillatory illumination vs STED microscopy. (a) In STED microscopy, a sample is imaged by collecting fluorescence from a small subwavelength spot of the sample, which must contain a fluorescent label. The fluorescent spot (bright area in the center of the gray disk) is surrounded by a larger dark area where fluorescence is depleted by intense laser radiation (orange disk). (b) In superoscillatory imaging, a sample is imaged by collecting the light scattered from a small area illuminated by the light focused into a subwavelength superoscillatory spot (bright spot in the center of a bigger halo).

REALIZATION OF THE MICROSCOPE WITH SUPEROSCILLATORY ILLUMINATION

Development of the superoscillatory microscope is underpinned by the design of the superoscillatory illumination. In principle, any prescribed, arbitrarily small superoscillatory focus can be constructed as a series of circular prolate spheroidal wavefunctions, S_i , which are band limited to $|k_0| \leq 2\pi/\lambda$.^{24,31} They form a complete orthogonal set over both the prescribed field of view and across the entire focal plane. However, it could happen that the chosen superoscillatory focus may only be achieved with a low intensity of the hotspot and may need a long series of wavefunctions to approximate, resulting in a complex and difficult-to-construct superoscillatory generator. Instead of targeting a pre-determined hotspot, we employed a different, simplified, and more efficient strategy. Using a series of only two orthogonal circular prolate spheroidal wavefunctions (see Fig. 4), we looked at which foci could be obtained by carefully balancing the amplitude coefficients of the two wavefunctions and optimizing the outcome.³¹

In the superoscillatory microscope reported here, we used a superoscillatory hotspot constructed from two circular prolate spheroidal functions $E(r/\lambda) = 3.123S_2(r/\lambda) + S_3(r/\lambda)$, where r is

the radial distance from the hotspot center. Figure 4 shows sample superoscillatory hotspots that are readily achievable by tailoring the wavefront with just a pair of spatial light modulators that control the intensity and phase profile of the beam incident on an objective. Here, we denote the hotspot full width at half maximum as D .

The hotspot with a spot size of $D = 0.4\lambda$ (equivalent to using an NA of 1.25) was used for imaging to achieve a compromise between the resolution and the throughput light efficiency of focusing, which affects the achievable frame rate of the instrument. In comparison, an ideal conventional lens of the same numerical aperture (NA = 1.0) as the focusing lens would create a diffraction-limited focal hotspot of 0.50λ .

A superoscillatory microscope can be constructed by adding a laser-based superoscillatory illumination system to a conventional microscope. We used an epi-fluorescence microscope equipped with a confocal module as the platform for our superoscillatory microscope. Superoscillatory illumination of the object can be achieved either by using a static superoscillatory lens^{32,33} or by shaping the input wavefront with spatial light modulators.^{29,34–36} The second approach, used in our instrument, has the advantages of allowing fast and easy reconfiguration of the hotspot, adaptive correction of instrumental imperfections in the optical path,³⁷ and enabling high-speed beam scanning. A sequence of two spatial light modulators allowed the conversion of the input laser beam ($\lambda = 488$ nm, Spectra-Physics Excelsior® One™ CW Laser) with a Gaussian profile into a carefully balanced superposition of two circular prolate spheroidal wavefunctions to achieve the superoscillatory focus. An oil immersion microscope objective with effective NA = 1.0 was used to focus the beam into a superoscillatory hotspot on the living cell through a coverslip, which was scanned using a pair of mirrors. Light scattered from the object was imaged by the same objective onto a pinhole and photomultiplier tube, the signal from which was used to record the image. The entire system, including spatial light modulators, scanning mirrors, and detector, was computer controlled. We have achieved superoscillatory imaging at a rate of 30 frames/s over a 512×512 pixel image.

To deliver sufficient image contrast from transparent fixed or living biological samples, we combined superoscillatory imaging with polarization contrast enhancement.^{38,39} Polarization microscopy in biological applications depends on local anisotropy and, since the earliest work by Schmidt⁴⁰ and Inoue,⁴¹ has been used to illustrate the dynamic complexity of cellular substructures

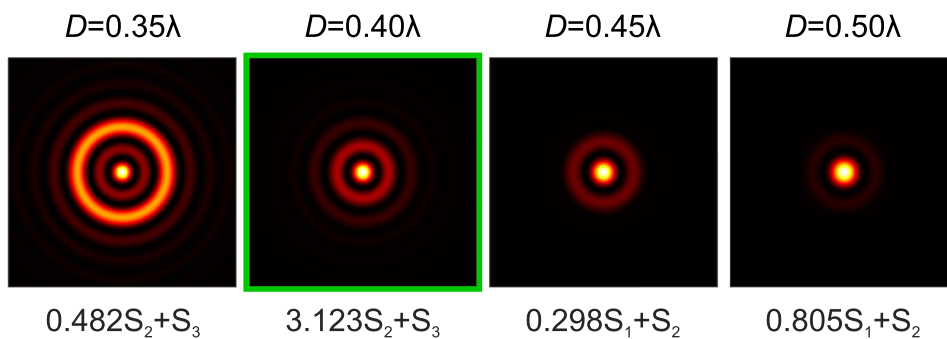


FIG. 4. Engineering of superoscillatory hotspots. A range of superoscillatory spots showing the flexibility of the design algorithm with a varying spot size. The superoscillatory spot used in the biological imaging is highlighted in green. Below each spot is the equation describing the construction of the spot from circular prolate spheroidal wavefunctions.

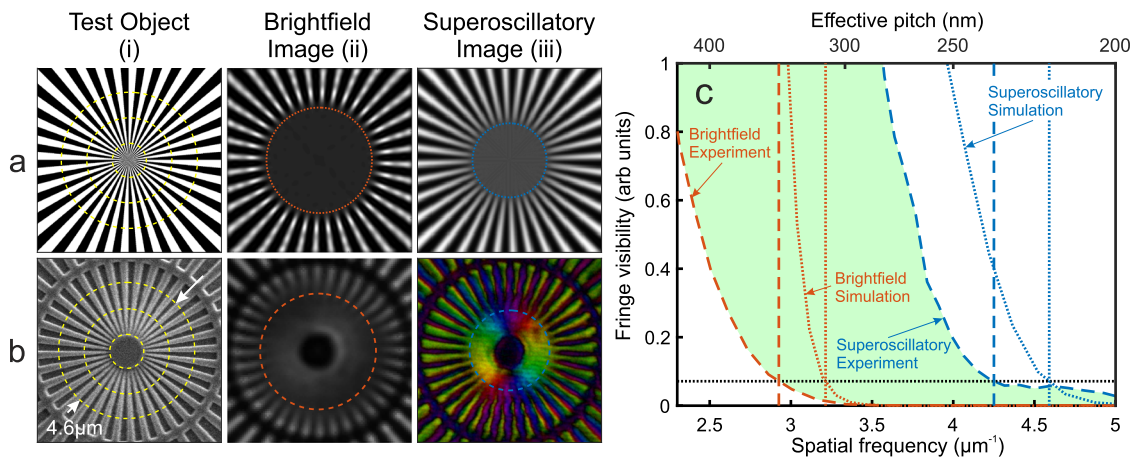


FIG. 5. Imaging the Siemens star. Panels (a) and (b) show images of a 36-sector binary Siemens star test object: (a/i) test sample design and (b/i) SEM image of the sample (40 nm chromium film on the glass substrate structured with a focused ion beam); (a/ii) simulated and (b/ii) experimental brightfield images with a conventional lens; (a/iii) simulated and (b/iii) experimental superoscillatory images with polarization contrast. See the text for the description of the false-color scheme used in (c/iii). Yellow dashed circles in (i) are for scale and have diameters of 1.1 μm , 2.9 μm , and 4.6 μm . Circles in (ii) and (iii) show resolution limits with line styles matching panel (c). Panel (c) shows spatial spectra of conventional brightfield images and superoscillatory images of the Siemens star [dashed lines—experiment, dotted lines—computer simulation; vertical dashed (dotted) lines show the limits of resolution in experiment (simulation)]. The resolution threshold is shown by the black dotted line. Note the radical increase in high-frequency components in the superoscillatory spectrum, in contrast to brightfield, making fine details of the image visible.

in living systems.^{42–47} Four images were taken of the sample with a relative polarization azimuth of the illuminating beam at 0°, 45°, 90°, and 135°. By combining these images computationally, we can recover the local anisotropy of the sample at each

pixel, represented by the differences in reflection, R , and the incident polarization angle, φ , at which maximum light is reflected (see formulae in the [supplementary material](#)). For display in a color figure [Figs. 5(b-iii), 6(b), 6(c), 7(a), and 7(b)], information

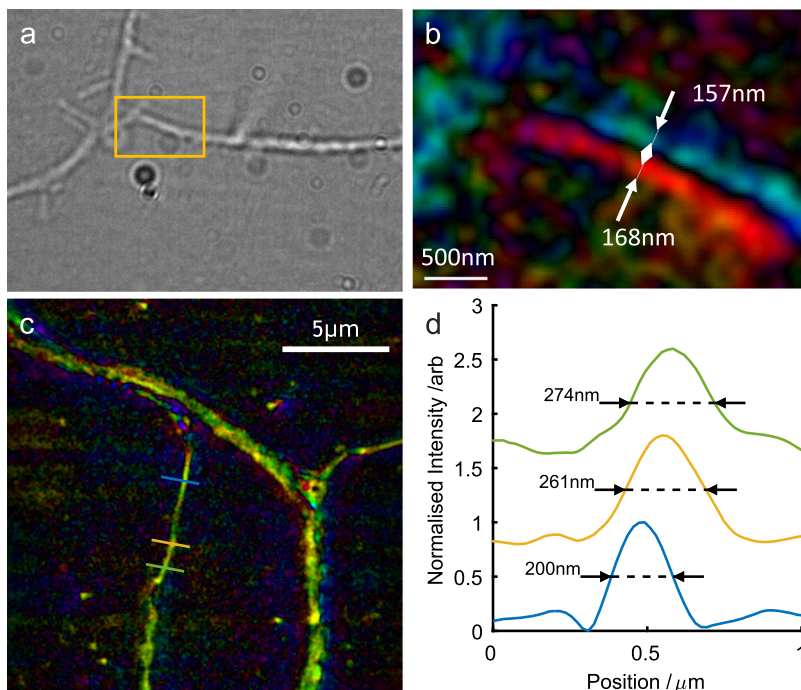


FIG. 6. Superoscillatory imaging of biological structures. Conventional brightfield image of a living neuronal process (a) and superoscillatory image of the region within the yellow box (b). See the text for the description of the false-color scheme used in (b) and (c). Panel (a) is deliberately slightly defocused to provide brightfield contrast in the transparent axon sample. Panel (c) shows the superoscillatory image of a live neuronal segment. Panel (d) shows the profiles along the lines shown in panel (c).

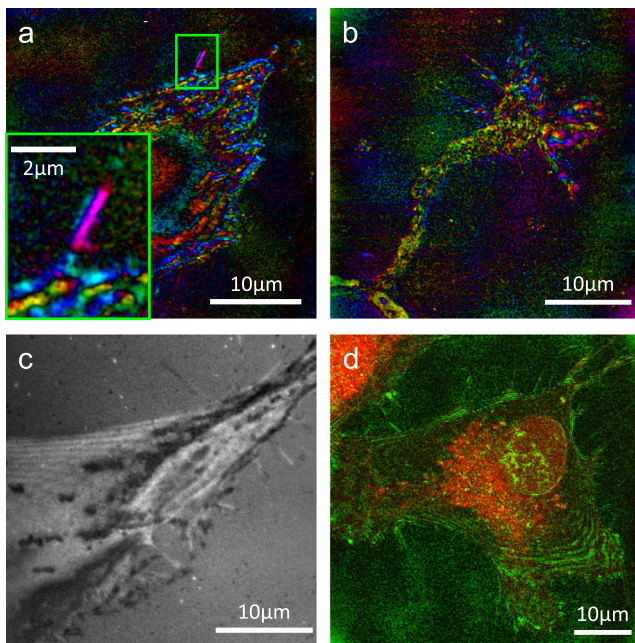


FIG. 7. Different modalities of superoscillatory imaging of living cells. (a) Superoscillatory polarization-contrast image of an unlabeled MG63 cell. The inset shows an enlargement of a filipodium. (b) Superoscillatory polarization-contrast image of a growth cone in an unlabeled mouse neuron. See the text for the description of the false-color scheme used in (a) and (b). (c) Non-polarized reflection-mode superoscillatory image of an unlabeled MG63 cell. (d) Superoscillatory image (magnitude only, green channel) combined with a confocal fluorescently labeled image (MitoTracker red, red channel) of an MG63 cell. (Multimedia view—see the [supplementary material](https://doi.org/10.1063/1.5144918.1) for details of the video.). Multimedia view: (a)–(d): <https://doi.org/10.1063/1.5144918.1>; <https://doi.org/10.1063/1.5144918.2>; <https://doi.org/10.1063/1.5144918.3>; <https://doi.org/10.1063/1.5144918.4>.

on R and φ is encoded such that brightness represents the magnitude of anisotropy R (on a linear scale normalized to the maximum anisotropy in the sample) and hue encodes the polarization azimuth φ . Thus, isotropic regions (those outside the sample for instance) are dark, where strongly anisotropic (highly structured) regions are bright. Polarization in the regions encoded in a particular hue (say, red) is aligned in the same direction.

IMAGING WITH THE SUPEROSCILLATORY MICROSCOPE

We tested the microscope resolution using a Siemens star, a recommended test pattern for super-resolution imaging⁴⁸ (Fig. 5). The superoscillatory microscope provides better transfer of the high-frequency components of the band-limited spectrum. This helps the visibility of fine structures in the Siemens star. With this type of sample, the key metric is how close to the center we can faithfully image. We see significantly increased sharpness in the superoscillatory image compared to the widefield image, particularly around the middle ($2.9 \mu\text{m}$) dashed yellow circle in (i), corresponding to a grating pitch of 250 nm as determined by the grating geometry.

To quantify the image improvement, we measure the fringe visibility around the circumference of a circle of decreasing radius in

the image. As the radius decreases, the pitch (or distance between grating lines) of the grating decreases and, hence, the spatial frequency increases. Figure 5(c) shows the variation of visibility with spatial frequency (lower scale) and effective pitch of the grating (upper scale) for simulated (dotted lines) and experimental (dashed lines) images. Simulation and experiment show very similar trends. The resolution is defined as the point at which the signal drops below a chosen threshold. We choose the threshold visually from the Siemens star images [Figs. 5(a) and 5(b)] by determining how far into the center the spokes are visible. We select the threshold as 0.07 units [black dotted line in panel (c)] and use this to determine the resolution in spatial frequency (lower scale) and nanometers (upper scale) for all plots. These resolutions are marked with vertical dotted/dashed lines in panel (c) and circles in (ii) and (iii). Superoscillatory microscope images achieve a perceived resolution of 235 [217] nm in experiment [simulation], which is a factor of 1.5 improvement over the 341 [311] nm resolution offered by brightfield imaging. Here, we note that the achieved resolution of 217 nm is close to the size of the illuminating superoscillatory hotspot $D = 0.4\lambda = 195 \text{ nm}$. The size of the hotspot is set experimentally and can be made smaller at the expense of transferring more energy to the sidebands. This spot size was chosen to demonstrate the super-resolution capability while maintaining high signal levels. In this setup, smaller spot sizes would reduce the signal and, hence, the achievable frame rate, but this can be easily compensated with a higher laser power than the $100 \mu\text{W}$ used here while staying well below the $1\text{--}10 \text{ mW}$ used in fluorescent confocal imaging.

We have also demonstrated imaging of biological samples. Imaging of biological samples has many challenges, beyond just achieving a good lateral resolution. Intense light can easily damage biological samples, and hence it is preferable to work at low illumination intensities. Superoscillatory imaging is, therefore, well placed, in contrast with STED imaging, for example, which inherently requires intensities above the saturation intensity of the fluorophore in use to achieve high resolutions. Indeed, in principle, superoscillatory focusing and imaging can be performed at arbitrarily low intensity levels, down to the level of single photon illumination.⁴⁹ Note also that the lack of an absorbing reporter in the sample significantly reduces any photo-toxic effects of the laser illumination, meaning that even in systems with a significant proportion of energy in the sidebands, total photon dose absorbed by the sample is much reduced. Live bioimaging also demands rapid image acquisition to capture dynamic processes. Our superoscillatory microscope uses scanning mechanisms similar to that of conventional confocal imaging and captures rates of up to 30 frames/s . However, bioimaging of transparent objects such as cells is complicated by a lack of intensity contrast, while optical anisotropy commonly occurs through molecular structuring.^{42,43} To improve imaging of such samples, we use polarized superoscillatory illumination to add anisotropy contrast to superoscillatory images and remove the need for fluorescent labeling, as described above.

To demonstrate biological imaging, we image both relatively well-known structures, where resolution measures can be taken (Fig. 6), and more complex living cellular systems (Fig. 7) (Multimedia view) with a range of scales and morphologies. We provide exemplar still images in this paper: equivalent videos of the live systems can be found in the [supplementary material](https://doi.org/10.1063/1.5144918.1). Figure 6(b) shows

a section of a single living neuronal process [panel (a)—conventional brightfield: primary culture of a hippocampal neuron], the long thin outgrowth from the neuron used to form network connections in the brain. In panel (b) (superoscillatory polarization image), the two sides of the process are clearly resolved. The widths of the two lines measured as the full width at half maximum of a profile of the magnitude of anisotropy are 157 nm ($\lambda/3.1$) and 168 nm ($\lambda/2.9$), considerably below 298 nm, the diffraction limit of a conventional lens with the same NA (equal to 1) as our objective. Note also the very clear isotropic gap between the two sides of the process [panel (b)], showing a nanoscale change in the polarization structure of the process. Panel (c) shows an image of a similar live neuronal process, with profiles through the colored lines shown in panel (d). Knowledge about the structure and dynamics of these neuronal processes is important in understanding the changes that occur in neurodegenerative conditions such as Alzheimer's disease and dementia. It should be noted that interpreting these images is not simple. The interaction of the polarized light reflected from the boundaries of a highly inhomogeneous and anisotropic medium is complex and is further complicated by interference with the light reflected from the interface between the coverslip and the sample. For example, the change in the polarization direction (denoted by color) between the sides of the axonal process in Fig. 7(b) (Multimedia view) is counter-intuitive and requires further investigation. While the microscope does give quantitative polarization measurements of simple samples (as seen in Fig. 5), quantitative analysis of the anisotropy of biological samples, therefore, remains an open question and would require further experimentation with simplified biological preparations. Having said this, polarization remains a powerful tool for obtaining contrast in unlabeled samples and has been shown to reveal interesting and biologically important information in similar preparations.^{50,51}

As a demonstration of further applications of the superoscillatory microscope, we have imaged different cell types using the different modalities of our instrument (Fig. 7) (Multimedia view). We have opted to study morphologically and ultrastructurally distinct cells of the nervous and skeletal systems as they are routinely investigated using conventional microscopy. Figure 7(a) (Multimedia view) shows a live image taken by the superoscillatory microscope of an unlabeled MG63 cell (human bone cell line), with the zoomed-in image detailing a single filopodium: an actin-filled protrusion used by the cell in its migration across the coverslip. Cancer cells are known to have modified migratory behavior, making the study of these systems highly relevant. Panel (b) shows the growth cone of an unlabeled mouse hippocampal neuron, where the characteristic fan shape is seen in great detail. The growth cone, at the leading tip of growing neuronal connection, determines how neurons form the networks that underlie functionality of the brain. Both the images of the bone cell and the growth cone exhibit a complexity from subcellular anisotropic structures. Such complexity is to be expected from earlier Polscope^{34,35} studies and 3D electron tomography of fixed cells, such as the immortalized pancreatic beta cell line, HIT-T15.⁵²

In Fig. 7(c) (Multimedia view), we show a non-polarized superoscillatory reflection image of an unlabeled MG63 cell taken from a real-time video captured at 3 frames/s. This also shows filopodia and superoscillatory spatial resolution but not the super-resolution of the anisotropic complexity exhibited in panel (a). It does

demonstrate an additional mode of the superoscillatory microscope. This type of reflection-mode imaging goes beyond the conventional resolution, which is very helpful in understanding the adhesion of cells to surfaces, which are key regulators of cell behavior and inter-cell signaling.

In addition to the novel polarization-contrast imaging, the fact that we have developed our microscope on a conventional confocal platform allows simultaneous capture of fluorescent images, enabling the correlative microscopy that is becoming increasingly important in biological imaging. Figure 7(d) (Multimedia view) shows a two-color image where the green channel shows the magnitude of anisotropy with the superoscillatory resolution and the red channel shows diffraction-limited confocal fluorescence from MitoTracker (a live-cell-compatible mitochondrial reporter). Images such as these allow us to unpick the detail of the polarization coding and eventually determine which biological structures cause the polarization signal, giving insight into cellular dynamics.

Collectively, these images show living cells in real time with minimal perturbation. They demonstrate how the superoscillatory instrument may be applied across a range of important biomedical areas, revealing new information in critical areas of study, such as the biomechanics of cancer and the mechanisms of neuronal dysfunction.

CONCLUSIONS

Our paper reports new label-free biological imaging that beats in resolution all other label-free techniques. We provide, for the first time, a mathematical description of a super-resolution imaging apparatus exploiting superoscillatory illumination of the sample with confocal detection of the image formed by a conventional lens. We show that super-resolution can be achieved by this band-limited optical instrument because the obtained image is a two-dimensional superoscillatory function. Hence, the spatial resolution of our microscope is set by the size of the superoscillatory hotspot and can break the Abbe-Rayleigh diffraction limit. We demonstrate that the local spatial resolution of a superoscillatory imaging system depends on the size of a superoscillatory hotspot that, in principle, can be arbitrarily small. We outline the construction of an imaging apparatus that is a modification of a conventional commercial optical microscope where conventional illumination is replaced with beam-shaping optics based on spatial light modulators. We show that our microscope can image minimally perturbed living cells with super-resolution at video frame rates, allowing new insights into their biological function. Finally, we show the potential for correlative microscopy where super-resolution polarized microscopy can be combined with standard fluorescence-based confocal detection, promising an avenue to identify the biological structures behind the complex anisotropic features recorded.

Superoscillatory polarization-contrast imaging is a new approach in the fundamentally important quest for ever-higher resolution biological imaging with minimal perturbation of a sample. Using standard Siemens star resolution test patterns, we have demonstrated a resolution close to the size of the illuminating superoscillatory hotspot and a factor of 1.5 better than that of bright-field imaging. Moreover, we show that this resolution can be translated into biological samples using laser powers 10–100 times lower than fluorescent confocal microscopes. The capabilities of our

microscope have been demonstrated on different cell types in different microscopy modalities, showing that it can work on a range of cell morphologies and scales and in a range of applications. The unique combination of advantages, unlabeled super-resolution, simple implementation, no *a priori* knowledge of the sample, and low phototoxicity, makes imaging with superoscillatory illumination a powerful tool for biological research and super-resolution imaging of samples that do not allow labeling, such as silicon chips. Finally, we note recent works that demonstrate that combining superoscillatory illumination⁵³ with artificial intelligence can lead to microscopy that beats the diffraction limit by two orders of magnitude.⁵⁴

SUPPLEMENTARY MATERIAL

See the [supplementary material](#) for a detailed description of the microscope construction, a comparison between confocal and superoscillatory imaging, and extended captions for the videos in [Fig. 7](#) (Multimedia view).

AUTHORS' CONTRIBUTIONS

E.T.F.R. and N.I.Z. conceived the superoscillatory microscope concept and developed the methodology of superoscillatory imaging to achieve super-resolution. P.J.S.S. and E.T.F.R. developed the idea of polarization-contrast superoscillatory microscopy. E.T.F.R. built the microscope and developed the associated software, captured the data, processed the images, and carried out the imaging simulations. K.S.R. and E.T.F.R. designed the superoscillatory spots. S.Q. and T.A.N. developed the live-cell culture techniques for superoscillatory imaging. T.A.N. supervised the cell-culture development. T.A.N. and P.J.S.S. selected the biological targets. E.T.F.R. and N.I.Z. wrote the manuscript. All authors discussed the results extensively and edited the manuscript. P.J.S.S. and N.I.Z. supervised and coordinated the work.

ACKNOWLEDGMENTS

This research was supported by Wessex Medical Research (Grant No. WMR03), the University of Southampton: Institute for Life Sciences and Enterprise Fund, the UK's Engineering and Physical Sciences Research Council (Grant No. EP/M009122/1), and the Singapore Ministry of Education [Grant No. MOE2016-T3-1-006 (S)].

The authors would like to thank Guanghui Yuan for numerous fruitful discussions; Alexander Buchnev and Jun Yu Ou for fabrication of the test masks; Grace Hallinan, Aleks Pitera, and Katrin Deinhardt for assistance with the neuronal cultures; Rudolf Oldenbourg for fruitful discussions; and Mark Willet of the Microscopy Facility in Biological Sciences at the University of Southampton for the matched fluorescent and DIC photos of HeLa cells used in [Fig. 3](#).

The authors declare no competing financial interests.

DATA AVAILABILITY

The data underlying this paper are available from the University of Southampton ePrints repository at <http://doi.org/10.5258/SOTON/D0598>. The Matlab code for processing and

analyzing the data is available upon reasonable request from E.T.F.Rogers@soton.ac.uk.

REFERENCES

- S. Y. Chou, P. R. Krauss, and P. J. Renstrom, *Appl. Phys. Lett.* **67**, 3114 (1995).
- S. J. McNab and R. J. Blaikie, *Appl. Opt.* **39**, 20 (2000).
- E. H. Synge, *Philos. Mag.* **6**, 356 (1928).
- D. W. Pohl, W. Denk, and M. Lanz, *Appl. Phys. Lett.* **44**, 651 (1984).
- A. Lewis, M. Isaacson, A. Harootunian, and A. Muray, *Ultramicroscopy* **13**, 227 (1984).
- J. B. Pendry, *Phys. Rev. Lett.* **85**, 3966 (2000).
- S. W. Hell, S. J. Sahl, M. Bates, X. Zhuang, R. Heintzmann, M. J. Booth, J. Bewersdorf, G. Shtengel, H. Hess, P. Tinnefeld, A. Honigmann, S. Jakobs, I. Testa, L. Cognet, B. Lounis, H. Ewers, S. J. Davis, C. Eggeling, D. Klenerman, K. I. Willig, G. Vicidomini, M. Castello, A. Diaspro, and T. Cordes, *J. Phys. D: Appl. Phys.* **48**, 443001 (2015).
- R. C. G. Smith, P. S. Stumpf, S. J. Ridden, A. Sim, S. Filippi, H. A. Harrington, and B. D. MacArthur, *Biophys. J.* **112**, 2641 (2017).
- M. T. Swilius and G. J. Jensen, *J. Bacteriol.* **194**, 6382 (2012).
- U. Schnell, F. Dijk, K. A. Sjollem, and B. N. G. Giepmans, *Nat. Methods* **9**, 152 (2012).
- M. G. Gustafsson, *J. Microsc.* **198**, 82 (2000).
- S. Chowdhury, A.-H. Dhalla, and J. Izatt, *Biomed. Opt. Express* **3**, 1841 (2012).
- B. Littleton, K. Lai, D. Longstaff, V. Sarafis, P. Munroe, N. Heckenberg, and H. Rubinsztein-Dunlop, *Micron* **38**, 150 (2007).
- D. Ruh, J. Mutschler, M. Michelbach, and A. Rohrbach, *Optica* **5**, 1371 (2018).
- F. Jünger, P. V. Olshausen, and A. Rohrbach, *Sci. Rep.* **6**(1), 30393 (2016).
- M. Piliarik and V. Sandoghdar, *Nat. Commun.* **5**, 4495 (2014).
- J. Ortega-Arroyo and P. Kukura, *Phys. Chem. Chem. Phys.* **14**, 15625 (2012).
- N. Shapira, Z. Deng, R. Remez, D. Singh, E. Katzav, and A. Arie, *Opt. Express* **27**, 34530 (2019).
- J. M. Guerra, *Appl. Phys. Lett.* **66**, 3555 (1995).
- G. T. Di Francia, *Nuovo Cimento* **9**, 426 (1952).
- Y. Aharonov, D. Z. Albert, and L. Vaidman, *Phys. Rev. Lett.* **60**, 1351 (1988).
- M. V. Berry and S. Popescu, *J. Phys. A: Math. Gen.* **39**, 6965 (2006).
- F. M. Huang, N. I. Zheludev, Y. Chen, and F. Javier Garcia de Abajo, *Appl. Phys. Lett.* **90**, 091119 (2007).
- F. M. Huang and N. I. Zheludev, *Nano Lett.* **9**, 1249 (2009).
- E. T. F. Rogers, J. Lindberg, T. Roy, S. Savo, J. E. Chad, M. R. Dennis, and N. I. Zheludev, *Nat. Mater.* **11**, 432 (2012).
- A. M. H. Wong and G. V. Eleftheriades, *Sci. Rep.* **3**, 1715 (2013).
- G. H. Yuan, K. S. Rogers, E. T. F. Rogers, and N. I. Zheludev, *Phys. Rev. Appl.* **11**, 064016 (2019).
- G. H. Yuan, E. T. F. Rogers, and N. I. Zheludev, *Light: Sci. Appl.* **8**, 2 (2019).
- S. Kosmeier, M. Mazilu, J. Baumgartl, and K. Dholakia, *J. Opt.* **13**, 105707 (2011).
- T. Wilson and C. J. R. Sheppard, *Theory and Practice of Scanning Optical Microscopy* (Academic Press (London) Ltd., London, UK, 1984).
- K. S. Rogers, K. N. Bourdakos, G. H. Yuan, S. Mahajan, and E. T. F. Rogers, *Opt. Express* **26**, 8095 (2018).
- E. T. F. Rogers, S. Savo, J. Lindberg, T. Roy, M. R. Dennis, and N. I. Zheludev, *Appl. Phys. Lett.* **102**, 031108 (2013).
- G. H. Yuan, E. T. F. Rogers, T. Roy, and N. I. Zheludev, *Opt. Express* **22**, 6428 (2014).
- J. Baumgartl, S. Kosmeier, M. Mazilu, E. T. F. Rogers, N. I. Zheludev, and K. Dholakia, *Appl. Phys. Lett.* **98**, 181109 (2011).
- M. A. A. Neil, R. Juškaitis, T. Wilson, Z. J. Laczik, and V. Sarafis, *Opt. Lett.* **25**, 245 (2000).
- M. Martinez-Corral, P. Andres, C. J. Zapata-Rodriguez, and C. J. R. Sheppard, *Optik* **107**, 145 (1998).
- M. J. Booth, *Light: Sci. Appl.* **3**, e165 (2014).

- ³⁸A. Le Gratiot, M. Dubreuil, S. Rivet, and Y. Le Grand, *Opt. Lett.* **41**, 4336 (2016).
- ³⁹S. B. Mehta, M. Shribak, and R. Oldenbourg, *J. Opt.* **15**, 094007 (2013).
- ⁴⁰W. J. Schmidt, *Chromosoma* **1**, 253 (1939).
- ⁴¹S. Inoué, *Chromosoma* **5**, 487 (1953).
- ⁴²K. Katoh, K. Hammar, P. J. S. Smith, and R. Oldenbourg, *Proc. Natl. Acad. Sci. U. S. A.* **96**, 7928 (1999).
- ⁴³K. Katoh, K. Hammar, P. J. S. Smith, and R. Oldenbourg, *Mol. Biol. Cell* **10**, 197 (1999).
- ⁴⁴N. M. Kalwani, C. A. Ong, A. C. Lysaght, S. J. Haward, G. H. McKinley, and K. M. Stankovic, *J. Biomed. Opt.* **18**, 026021 (2013).
- ⁴⁵J. C. M. Low, T. J. Ober, G. H. McKinley, and K. M. Stankovic, *Biomed. Opt. Express* **6**, 599 (2015).
- ⁴⁶E. J. Jáuregui, O. Akil, C. Acevedo, F. Hall-Glenn, B. S. Tsai, H. A. Bale, E. Liebenberg, M. B. Humphrey, R. O. Ritchie, L. R. Lustig, and T. Alliston, *Bone* **89**, 7 (2016).
- ⁴⁷C. B. Raub, S. C. Hsu, E. F. Chan, R. Shirazi, A. C. Chen, E. Chnari, E. J. Semler, and R. L. Sah, *Osteoarthritis Cartilage* **21**, 860 (2013).
- ⁴⁸R. Horstmeyer, R. Heintzmann, G. Popescu, L. Waller, and C. Yang, *Nat. Photonics* **10**, 68 (2016).
- ⁴⁹G. H. Yuan, S. Vezzoli, C. Altuzarra, E. T. F. Rogers, C. Couteau, C. Soci, and N. I. Zheludev, *Light: Sci. Appl.* **5**, e16127 (2016).
- ⁵⁰G. Danuser and R. Oldenbourg, *Biophys. J.* **79**, 191 (2000).
- ⁵¹R. Oldenbourg, K. Katoh, and G. Danuser, *Biophys. J.* **78**, 1176 (2000).
- ⁵²B. J. Marsh, D. N. Mastrorarde, K. F. Buttle, K. E. Howell, and J. R. McIntosh, *Proc. Natl. Acad. Sci. U. S. A.* **98**, 2399 (2001).
- ⁵³T. Pu, J. Y. Ou, N. Papisimakis, and N. I. Zheludev, *Appl. Phys. Lett.* **116**, 131105 (2020).
- ⁵⁴T. Pu, V. Savinov, G. Yuan, N. Papisimakis, and N. I. Zheludev, "Unlabelled far-field deeply subwavelength superoscillatory imaging (DSSI)," [arXiv:1908.00946](https://arxiv.org/abs/1908.00946) [physics.optics] (2019).